condensed matter

MDPI

Article

Detection of Spin Polarized Band in $VO_2/TiO_2(001)$ Strained Films via Orbital Selective Constant Initial State Spectroscopy

Alessandro D'Elia [1,2,*], Cesare Grazioli [1], Albano Cossaro [1,3], Bowen Li [4], Chongwen Zou [4], Seyed Javad Rezvani [1,5], Augusto Marcelli [6,7,8] and Marcello Coreno [8]

1 IOM-CNR, Laboratorio TASC, Basovizza SS-14, km 163.5, 34149 Trieste, Italy; grazioli@iom.cnr.it (C.G.); cossaro@iom.cnr.it (A.C.); seyedjavad.rezvani@unicam.it (S.J.R.)
2 II Physikalisches Institut, Universität zu Köln, Zülpicher Straße 77, 50937 Köln, Germany
3 Department of Chemical and Pharmaceutical Sciences, University of Trieste, via L. Giorgieri 1, 34149 Trieste, Italy
4 National Synchrotron Radiation Laboratory, University of Science and Technology of China, Hefei 230029, China; bowenli@mail.ustc.edu.cn (B.L.); czou@ustc.edu.cn (C.Z.)
5 Scuola di Scienze e Tecnologie, Sezione di Fisica, Università di Camerino, Via Madonna delle Carceri 9, 62032 Camerino, Italy
6 Istituto Nazionale di Fisica Nucleare, Laboratori Nazionali di Frascati, 00044 Frascati, Italy; augusto.marcelli@lnf.infn.it
7 Rome International Centre for Material Science Superstripes, RICMASS, Via dei Sabelli 119A, 00185 Rome, Italy
8 ISM-CNR, Istituto Struttura della Materia, LD2 Unit, Basovizza Area Science Park, 34149 Trieste, Italy; marcello.coreno@elettra.eu
* Correspondence: delia@iom.cnr.it

Received: 12 October 2020; Accepted: 9 November 2020; Published: 12 November 2020

Abstract: The VO_2 is a $3d^1$ electron system that undergoes a reversible metal–insulator transition (MIT) triggered by temperature and characterized by an interplay between orbital, charge and lattice degrees of freedom. The characterization of the MIT features are therefore extremely challenging and powerful investigation tools are required. In this work, we demonstrate how a combination of resonant photoemission and constant initial state (CIS) spectroscopy can be used as an orbital selective probe of the MIT studying three different $VO_2/TiO_2(001)$ strained films. The CIS spectra of the V *3d* and V *3p* photo-electrons shows sensitivity to different orbital contribution and the presence of a spin polarized band close to the Fermi level.

Keywords: strain; spin polarization; VO_2; orbital selective; constant initial state; resonant photoemission; band structure; metal-insulator transition

1. Introduction

The VO_2 is a fascinating system, well know from 60s for its metal–insulator transition (MIT). The transition is triggered by temperature (67 °C in bulk crystals) and since its discovery [1], it continuously attracted the attention of researchers because of possible applications in different areas as energy savings [2–4], electron correlation driven electronic devices and ultra-fast switching [5–7]. However, the nature of the MIT itself is determined by the complex interplay among lattice, electronic and orbital degrees of freedom [8–14], which make the transition feature highly dependent on sample quality and synthesis methods [15]. Consequently, different strategies have been applied in order to control and manipulate the MIT features like doping, application of epitaxial strain [11,13,16,17] and exploitation of quantum size effects [18–20]. Among them, strain emerges as a powerful method

to tune the MIT, since it modifies atomic distances, orbital order and, in particular, electron-electron correlation. X-ray absorption near edge structure (XANES) is particularly suitable to study the complex VO_2 scenario, since it is able to probe at the same time the electronic structure and the local order [21–26]. Since, in materials at low dimensions, the electronic properties can be modulated by different parameters, such as surface states and spatial confinement [27–31], the investigation of electronic configuration in strained VO_2 can lead to its exploitation in several applications.

In a previous work, we confirmed the reliability of XANES to probe the orbital strain dynamics across the MIT [17]. We probed the structural and orbital contributions by monitoring the changes in the V $L_{2,3}$ edge XANES on single crystalline strained films of VO_2/TiO_2 (001)

In this manuscript, we demonstrate that the combination with resonant photoemission spectroscopy (ResPES) allows us to collect and identify XANES partial electron yield spectra connected to the different screening channel of the VO_2 valence band [32]. This is possible because ResPES offers the possibility to change the photon energy through a resonance of the system, therefore, probing the resonant behavior of photoemission spectra.

The intensity of the photoemission spectra is modulated because of the interference between the direct photoemission channel and the photoabsorption Auger-like channels. Two acquisition methods can be considered to study the resonance effect: constant final state (CFS) and constant initial state (CIS) spectroscopy [33]. In the constant final state, the spectrum is collected when the incident photon energy hv varies while the detected electron kinetic energy is constant [21,33,34]. XANES spectra acquired with the Auger yield is the typical example of the CFS acquisition. The strength of the CFS spectroscopy relies on the possibility to choose the appropriate Auger channel to probe the system. As demonstrated in previous studies selecting the Auger V $L_3M_{23}M_{45}$ or the O $KL_{23}L_{23}$, it is possible to optimize the collection at the vanadium L edges, or at the oxygen K edge in any vanadium oxide [17,22,35].

In a CIS acquisition, both the energy of the exciting photon and the energy of the detected photoelectron (Ke) are simultaneously varied, in order to maintain constant the binding energy (BE) = hv − K_e [21,33,34]. ResPES spectra are collected using the CIS mode to probe the same binding energy region for each photon energy. As a consequence, CIS spectroscopy allows studying the resonant enhancement of the cross-section of a selected photoemission feature when the photon energy spans through a core resonance. In synthesis, CIS and CFS are two detection methods, which allow for the collection of an absorption spectrum exploiting different XANES partial electron yield channels.

This work focuses on CIS absorption spectra of *3d* and *3p* electrons in VO_2. Tuning the photon energy through the *2p* core resonance, different possible decays of the excited state have been measured [36]. In our case the absorption process results in the excitation

$$2p^6 3d^1 + h\nu \rightarrow 2p^5 3d^2 \quad (1)$$

which can decay via the Coulomb interaction in two configurations with the emission of one electron from different vanadium and oxygen orbitals:

$$2p^5 3d^2 \rightarrow 2p^6 3d^0 + e_d \quad (2)$$

$$2p^5 3d^2 \rightarrow 2p^6 3p^5 3d^1 + e_p \quad (3)$$

The processes described by Equations (2) and (3) emit a *3d* and a *3p* electron, respectively, and in the ResPES spectra, they will constructively interfere with *3d* and *3p* direct photoemission channels. The samples investigated were three strained VO_2/TiO_2 films (8 nm, 16 nm and 32 nm thick). We demonstrated that, by exploiting the extreme selectivity of the CIS spectroscopy, it has been possible to probe the strain induced orbital dynamic across the MIT with orbital selectivity and, as a consequence, obtained new insights on the spin polarization of the electronic structure of VO_2.

2. Results

2.1. V 3d CIS Spectroscopy

The quality of the three strained films of 8 nm, 16 nm and 32 nm thickness has been verified through temperature dependent resistivity (reported in Figure A1 in Appendix A for sake of brevity).

The resistivity curves show hysteresis loop with a thickness dependent transition temperature ~315 K in the 8 nm film, ~330 K in the 16 nm and ~345 K in the 32 nm film, in agreement with the thickness dependent transition temperature reported in previous studies [11].

The major spectral changes across the MIT in VO_2 occur around the Fermi level (FL) involving mainly V *3d* electrons. The oxygen atoms are locally arranged around the central V atom, according to the slightly distorted octahedral geometry. The t_{2g} and e_g manifold is split in three main bands: σ* and π*, which are generated by the chemical bonds among V *3d* and O *2p* electrons with σ and π symmetry, respectively, and the $d^*_{||}$ band, populated by unpaired *d* electrons [37] (See Figure 1).

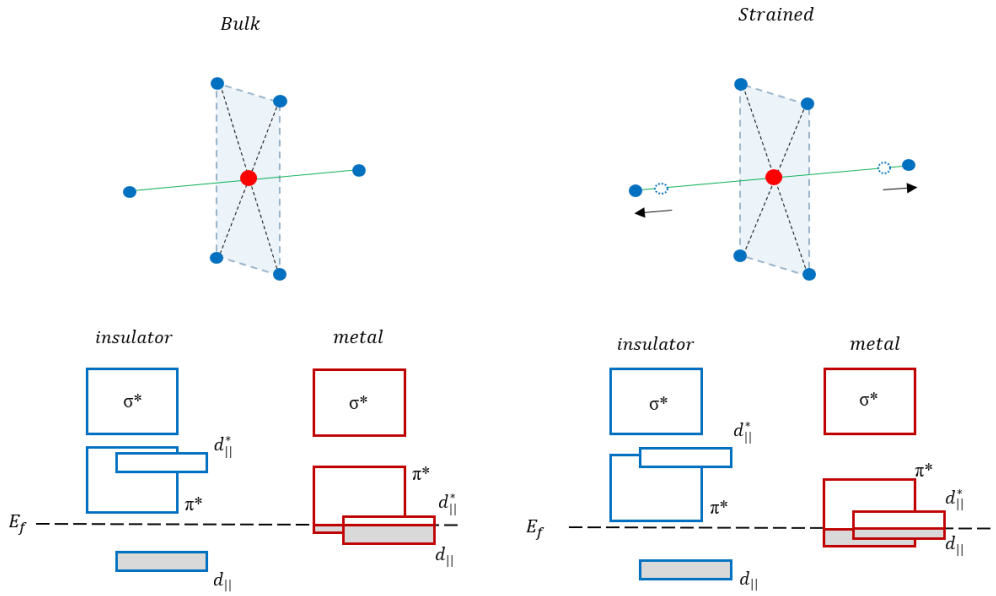

Figure 1. Schematic representation of the effect of the strain over the ligand environment and the band structure in the low and high temperature phases of VO_2 (see text for more details). Blue circles represent oxygen atoms, while the red represent vanadium atoms.

Across the phase transition π* and $d^*_{||}$ collapse to the FL becoming partially populated. Using the TiO_2(001) as the substrate, the effect of the tensile strain is that of increasing the apical oxygen-vanadium distances. This reduces the stability of the π* band which, in the metallic phase, is a downshift in energy, while the $d^*_{||}$ band is upshifted [11,17]. The overall effect is the inversion of orbital population at the FL (See Figure 1).

The Valence Band (VB) photoemission spectral features of the VO_2 can be described in terms of the final state configurations. In the insulating phase, the V *3d* peak is centered at ~1.5 eV, as can be seen from Figure 2 (an example of single VB spectra acquired at different photon energy can be found in Figure A2 in Appendix B).

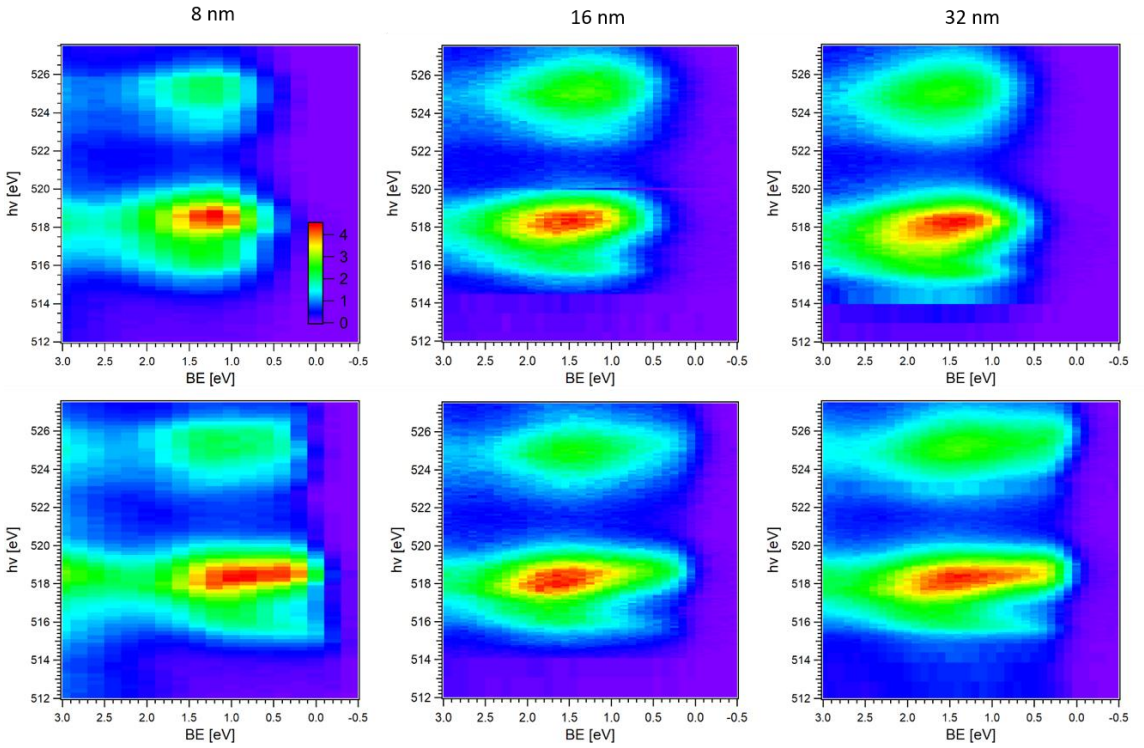

Figure 2. Resonant photoemission spectroscopy (ResPES) maps of the V *3d* electrons (binding energy (BE) region −0.5; 3 eV) across the L_3 (~518.2 eV) and L_2 (~526 eV) resonances. The energy range of the maps is hv [512–527.5] eV. All maps of the samples (8 nm, 16 nm and 32 nm) are vertically aligned with the top panels referring to the insulating phase and the bottom panels to the metallic phase. The color bar indicates the intensity scale: blue for low intensity and red for high intensity.

Its nature can be explained assuming that the V *3d* photo-hole is locally screened by the oxygen atoms around the metallic V atom at the center of the octahedral configuration (see Figure 1). Therefore, the final state is depicted as the $3d^1\underline{L}$ (ligand hole) [32]. In the metallic state, we assist the population of the FL. Since electrons are free to move within the solid, an additional screening mechanism and, therefore, an additional final state is available, and can be recognized in the VB: the $3d^1\underline{C}$ (coherent hole). This is generated by the non-local screening channel of the photo-hole provided by the surrounding vanadium atoms, and it is centered at about 0.4 eV [32].

Since $\underline{C}$ and $\underline{L}$ VB features are generated by two different screening mechanisms, they couple differently with the resonant excited state and exhibit a different CIS lineshape. For the metallic phases (bottom panels of Figure 2) it is easily recognized the population at the FL at BE = 0 eV. The maximum of the resonance is located in the energy range 518 to 519 eV. At hv ~516 eV a weaker resonant enhancement is also observed. The photon energy of the V *3d* electrons is more pronounced across the L_3 edge with respect to the L_2, because of the presence of Coster–Kronig decay (V $L_2L_3M_{4,5}$) [38]. Therefore, we limited the study of the spectral changes to the L_3 edge.

The CIS spectra of the $\underline{C}$ valence band feature are compared in Figure 3. All spectra have been normalized to the maximum of the L_3 resonance intensity. In the metallic phase, two main features are clearly detected, the σ* resonance around 518.4 eV and the small pre-edge peak at ~516 eV.

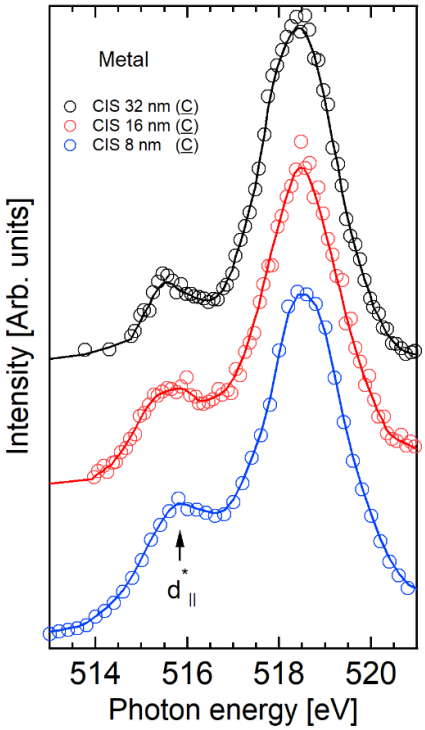

Figure 3. Comparison of constant initial state (CIS) spectra of the C valence band feature (0.4 eV) in the metallic phase for the 32 nm, 16 nm and 8 nm thick films in the photon energy range: 513–521 eV. The circles are the experimental points while the continuous lines are smoothed curves (binomial algorithm) used as guides for the eye.

The CIS spectra resemble the more commonly studied XANES spectra that also exhibit a strong σ* resonance and a pre-edge peak feature [17]. In XANES spectra collected across the phase transition boundaries, the most evident spectral changes are observed in the pre-edge peak region, which is mostly generated by a superposition of π* and $d^*_{||}$ bands [22,39,40], as demonstrated for this set of film in our previous study [17]. However, since XANES is less selective than CIS, the line-shape is usually broader, and the pre-edge peak is not well isolated, as in Figure 3. Since CIS is a XANES partial electron yield, across the MIT, we expect to observe the same behavior as XANES, i.e., spectral changes around the pre-edge energy region. However, an increased sensitivity to different spectral feature as a function of the CIS channel is expected.

To understand the nature of the CIS pre-edge peak, it is necessary to follow its evolution vs. thickness, i.e., the strain contribution. Increasing the strain, the intensity of the pre-edge peak increases relatively to the σ* resonance, and concurrently, the valley amongst them decreases its deepness. In addition, a broadening of the pre-edge peak width occurs. In the metallic phase of the VO_2, π* and $d^*_{||}$ are partially degenerate at the FL and, hence, are both populated, although with a different occupation. In bulk VO_2, because of the strong V-O hybridization, the FL is mostly occupied by the $d^*_{||}$ band with a small component of π* (see Figure 1). In strained samples the $d^*_{||}$ band empties respect to the π* band, opposite to bulk samples. As a consequence, it is possible to assign the pre-edge peak of the C CIS spectra in the metallic phase to the $d^*_{||}$ band (516 eV). In fact, its intensity and width increase with the strain, indicating that the increase of the empty states in agreement with the strain-induced orbital dynamics described above. In addition, within our experimental resolution, any spectral feature linked to the π* band are not detectable. It is important to notice that, with respect to standard XANES spectra, the increased selectivity of CIS spectroscopy make it possible to collect spectra with sharper features.

The CIS spectra of the L valence band feature (BE = 1.5 eV) are compared in Figure 4. The overall line shape is broader in respect to the C CIS spectra, and the individual orbital contributions are not distinguishable. In the metallic phase, the feature at ~516 eV is evident.

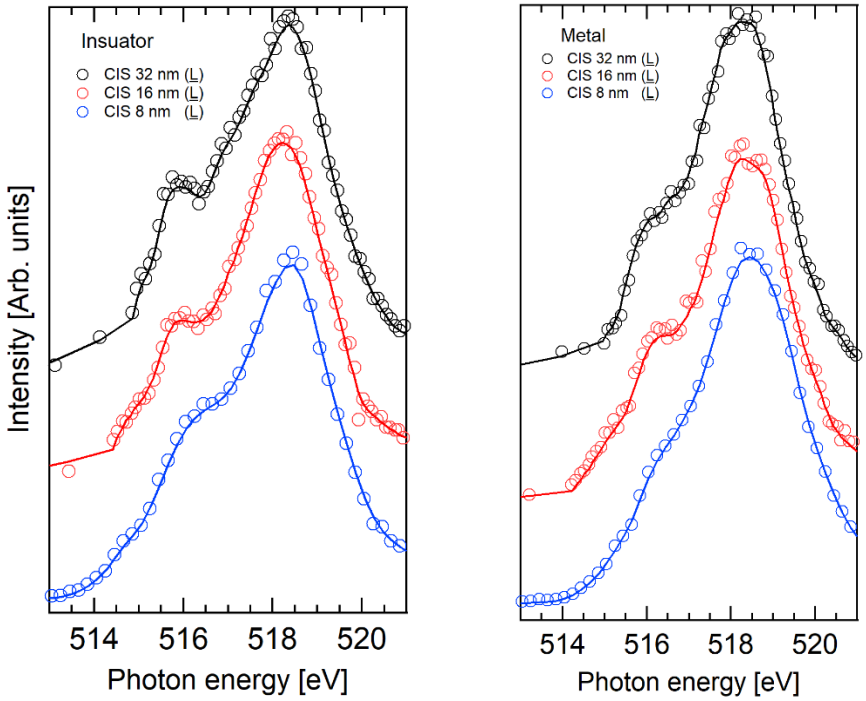

Figure 4. Comparison of CIS spectra of the L valence band feature (1.5 eV) in the insulating (**a**) and in the metallic phase (**b**) for the 32 nm, 16 nm and 8 nm thick films in the photon energy range 513–521 eV.

Increasing the strain, its intensity decreases. This trend is compatible with the increase of the population (and the depletion of the empty states) of the π* band as a function of the strain, which suggests an increased π* sensitivity in respect to the CIS spectra of the C feature. In the insulating phase, the feature around 515.5 eV is assigned to the π* band. The $d^*_{||}$ band is not detectable, because of the broadening of the σ* features, which might cover this weak signal.

The selective sensitivity to different empty bands for the C and L partial electron yield is due to their nature. The C final state is generated by the cooperative screening of the *3d* photo hole by the nearest vanadium atoms. In metallic vanadium dioxide, the $d^*_{||}$ band is directed along the rutile c axis, i.e., along the V-V bonds. These intermetallic bonds are the same as those involved in the non-local screening mechanism of the C final state, therefore, it is very likely that the core-hole excited state $2p^5 3d^2$ wave function (where the extra *3d* electron lies in the $d^*_{||}$ band) has a greater overlap with the $3d^1$C final state wave function. The same consideration can be applied to explain the higher sensitivity of the L CIS spectra to the π* empty band. In the L final state, the *3d* photo hole is locally screened by oxygen atoms of the octahedral coordination. Since the π* band is formed by V *3d* electrons, which form bonds with π character with oxygen atoms, an excited electron lying in the π* band is more likely to be spatially close to oxygen atoms. Then, the Auger transition of the excited state with an extra electron in the π* band is favored in the L final state.

2.2. V 3p CIS Spectroscopy

In addition to the *3d* electrons, we investigated the resonating behavior of the V $3p_{1/2}$ and $3p_{3/2}$ electrons (Equation (3)) across the V L_3 edge. V *3p* electrons can be found at ~41 eV of BE (see Figures 5 and A3 in Appendix B). The lineshape is quite broad, since the multiplet effect

splits V *3p* levels in two components: V $3p_{1/2}$ and $3p_{3/2}$, similarly to V *2p* electrons. In this case, however, the spin-orbit splitting is quite small, and a fitting procedure is necessary to separate the two contributions. The V $3p_{1/2}$ and $3p_{3/2}$ components have been modelled using a pseudo-Voigt curve [41] fixing their intensity ratio to 0.5, while for the background, a Shirley curve has been used. The fit returns the V $3p_{1/2}$ component at BE = 43.6 eV and the $3p_{3/2}$ at BE = 41.2 eV. The measured spin–orbit splitting (2.4 eV) is higher in respect to the value of 1 eV estimated by Zimmerman and co-workers [42].

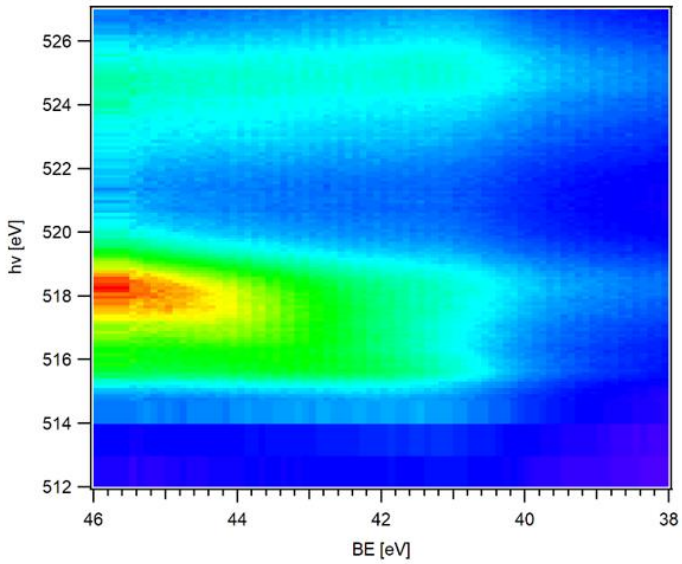

Figure 5. V *3p* ResPes map of the sample of 32 nm thickness in the insulating phase. The map was collected in the photon energy range hv = 512–527 eV across the V L_3 (~518 eV) and L_2 (~526 eV) resonances. The color bar indicates the intensity scale: blue for low intensity and red for high intensity.

Exploiting these results, the CIS spectra of the $3p_{1/2}$ (BE = 43.6 eV) and $3p_{3/2}$ (BE = 41.2 eV) features have been obtained. For the sake of brevity, the CIS spectra of the $3p_{1/2}$ and $3p_{3/2}$ components are called $CIS_{1/2}$ and $CIS_{3/2}$, respectively. The $CIS_{3/2}$ spectra are compared in Figure 6, and the contribution to the intensity of the V *3p* CIS spectra of the incoherent Auger channel V $L_3M_{23}M_{45}$ has been minimized using the procedure in [43].

The V $3p_{3/2}$ spectra exhibit a strong enhancement of the pre-edge feature respect to the V *3d* CIS spectra. This is due to the large overlap among *3p* and *3d* orbitals, which may favor the decay $2p^5 3d^2$ -> $2p^6 3p^5 3d^1$ + e_p of the photo-excited state. According to the analysis of the V *3d* CIS spectra, the two features of the $CIS_{3/2}$ spectra of the metallic phase can be assigned to the $d^*_{||}$ (515.8–516 eV) and σ* (518.4 eV) empty bands. In the metallic phase, their intensity ratio ($d^*_{||}$/σ*) increases with the strain, in agreement with the V *3d* (C) CIS spectra and the strain-induced orbital occupancy at the Fermi level, by shifting up the $d^*_{||}$ while lowering the π* band. In addition, the $d^*_{||}$ and σ* features are separated by about 2.5 eV, again, in good agreement with the $d^*_{||}$-σ*split observed in the *3d* C CIS spectra.

In the insulating phase, $d^*_{||}$ (515.9 eV) and σ* (518.3 eV) bands are separated by 2.4 eV, in agreement with XANES results available in the literature [44].

The $CIS_{1/2}$ spectra are compared in Figure 7. An unresolved feature is detected at ~516 eV and in the insulating phase, all spectra are dominated by two main features at 518.1 eV and at 516.7 eV. The energy position does not match that of the $d^*_{||}$ and σ* features observed in the $CIS_{3/2}$ spectra.

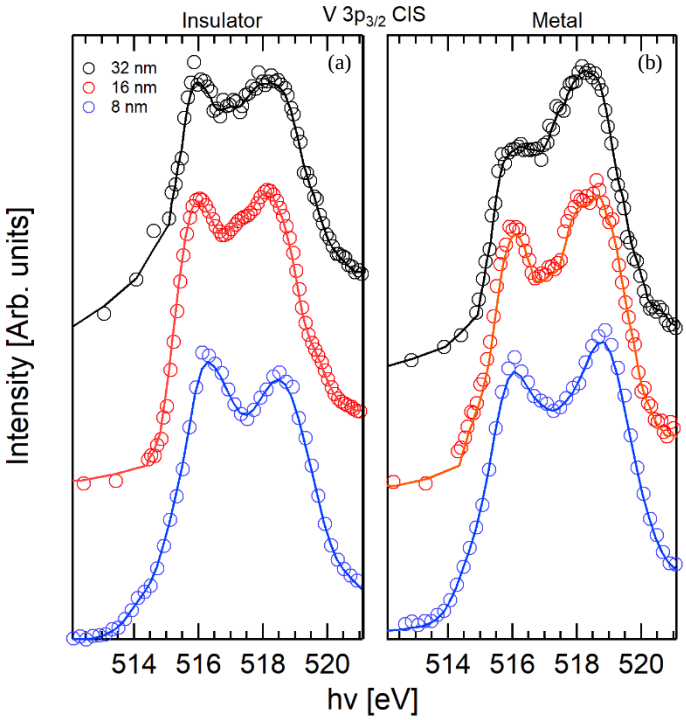

Figure 6. Comparison of $CIS_{3/2}$ spectra (BE = 41.2 eV) in the photon energy range 512.1–521.1 eV for the 32 nm, 16 nm and 8 nm thick films (black, red and blue lines, respectively). (**a**): The insulating phase spectra; (**b**): the metallic phase spectra.

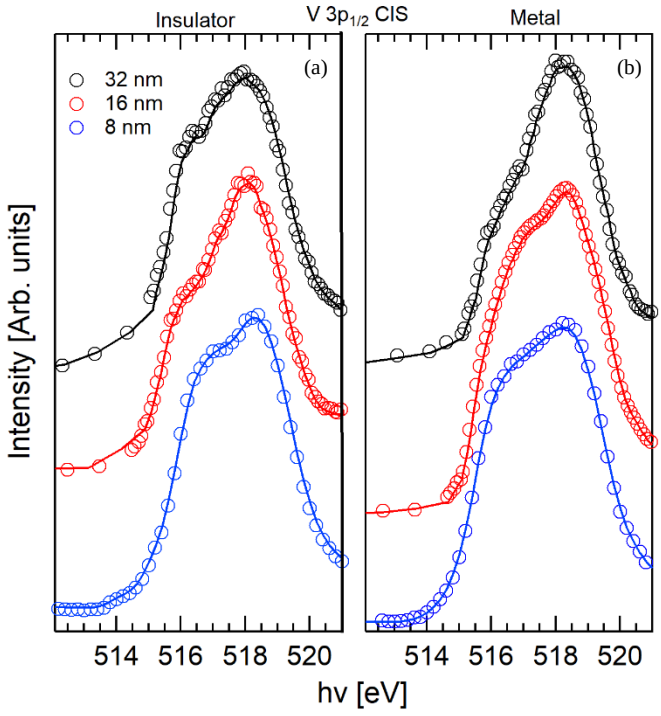

Figure 7. Comparison of $CIS_{1/2}$ (BE = 43.6 eV) spectra in the photon energy range 512.1–521.1 eV for the 32 nm, 16 nm and 8 nm thick films (black, red and blue lines, respectively). (**a**): the insulating phase spectra; (**b**): the metallic phase spectra.

The pre-edge peak of the $CIS_{1/2}$ spectrum is shifted toward higher energies respect to the $CIS_{3/2}$ spectra, indicating that the excited states associated to the Auger decay of the $3p^3{}_{3/2}$ and the $3p^1{}_{1/2}$

final states are different. At the resonance of the L_3 edge, the only electrons available for the XANES excitation are the $2p_{3/2}$. As a consequence, because of the dipole selection rules, the total angular momentum of the electron excited in the resonant state can only be J = 5/2 or J = 1/2. Depending on the J value, electrons can be excited in the specific empty band with the proper symmetry. This may result in a preferential decay of the excited state in the V $3p_{3/2}$ or $3p_{1/2}$, depending on the excited and final state symmetry.

In the $CIS_{3/2}$ spectra a huge increase in the $d^*_{||}$ band sensitivity is observed, while the $CIS_{1/2}$ does not show any resolved feature correlated to the MIT. This result suggests the occurrence of a spin polarization of the $d^*_{||}$ band, which favors the decay in the final state with a hole in the V $3p_{3/2}$ level.

3. Discussion

Our work demonstrates how the selectivity of CIS spectroscopy can be exploited, in order to track the strain induced orbital dynamic of VO_2 across the MIT and extract important information regarding the band structure.

The use of ResPes allowed us to isolate the contribution in the VB spectra from two different screening channel $\underline{L}$ and $\underline{C}$.

We showed that the CIS spectra of these two features are orbital selective probes of the empty bands structure of VO_2 as a function of strain and across the MIT. In particular, the $\underline{C}$ CIS spectra are more selective toward the $d^*_{||}$ band while the $\underline{L}$ spectra to the π^*.

The $\underline{C}$ screening channel is generated by the cooperative screening of the photo-hole from itinerant electrons in metallic VO_2. Accordingly, the $\underline{C}$ CIS spectra exhibits a pronounced sensitivity for the $d^*_{||}$ band, which are related with the intermetallic bond. This allowed us to observe a progressive depopulation of the $d_{||}$ band at FL (increase in $d^*_{||}$ band intensity) as a function of strain.

On the other hand, for the $\underline{L}$ channel the photo-hole is screened by the nearest oxygen atoms. Consequently, the CIS spectra of the $\underline{L}$ feature show an increased sensitivity for the π^* band. As a function of strain, the reduction of the intensity of the π^* related feature is observed, which confirms the strain induced orbital evolution of the π^* band in the metallic phase of VO_2.

Finally, from the analysis of the CIS spectra of the *V 3p* electrons, we suggest the occurrence of the spin polarization of the $d^*_{||}$. The use of CIS spectroscopy as orbital selective probe of the MIT in VO_2 demonstrated in this study can be extended to all transition metal oxides and, in general, to many other complex or correlated systems.

4. Materials and Methods

VO_2 films 8 nm, 16 nm and 32 nm thick were deposited on a clean substrate of TiO_2 (001) using RF-plasma assisted oxide-MBE instrument with a base pressure $< 4 \times 10^{-9}$ mbar. Using a growth rate of 0.1 Å/s, the thickness was controlled via the deposition time. During the growth, the substrate was heated at the temperature of 550° C. Additional details of the epitaxial film preparation are reported elsewhere [11,45].

CIS and ResPes experiments were performed at the ANCHOR end-station of the ALOISA beamline [46] at the Elettra synchrotron radiation facility. The photoelectrons were collected at normal emission by a PSP Vacuum 120 mm electron analyzer equipped with a 2D delay line detector. The photons were linearly polarized in the scattering plane and the sample was irradiated at the magic angle (~35° respect to the sample surface). Measurements were performed using the constant pass energy of E_p = 20 eV with an overall resolution of 0.25 eV.

The ResPes maps of the 16 nm and 32 nm films were acquired using two different intervals of photon energy 511–514 eV (step 1 eV) and 514.2–528.2 eV (step 0.2 eV). The photoelectrons were acquired in the kinetic energy (KE) range 502–508 eV (step 0.1 eV) to collect the V *3d* photoemission signal, while to detect V *3p* photoelectrons, the KE 460–470 eV (step 0.2 eV) was used. For the 8 nm sample, the photon energy range was 511–528.2 (step 0.2 eV), V *3d* KE range 502–508 eV (step 0.25 eV)

and V *3p* (step 0.25 eV). In the next sections of this work, the spectra presented as metallic and insulating VO_2 have been acquired at temperatures of 90 °C and 25 °C, respectively, unless specified otherwise.

Author Contributions: Conceptualization, A.M., M.C.; methodology, A.D., A.C., C.G.; investigation, A.D., A.C., C.G., S.J.R.; data curation, A.D.; sample synthesis: C.Z., B.L. writing—original draft preparation, A.D.; writing—review and editing, A.D., A.M., A.C., C.G., J.R.; funding acquisition, M.C. All authors have read and agreed to the published version of the manuscript.

Funding: This research has been performed within the Elettra Proposal #20185279 "XANES and Res PES study of Metal Insulator Transition in VO_2 thin films." at the ALOISA beamline.

Conflicts of Interest: The authors declare no conflict of interest.

Appendix A

The quality of the films has been tested via resistivity measurements. The three orders of magnitude jump in resistivity and the transition width of about 15 K are fingerprints of good sample crystallinity [15].

The transition temperatures are ~315 K in the 8 nm film, ~330 K for the 16 nm and ~345 K in the 32 nm film. The decrease in transition temperature is due to the application of strain that slightly modifies the atomic positions. In particular, depositing VO_2 on TiO_2 (001) allows for the shortening of the V-V distances along the rutile c axis, modifying the orbital occupancy and, thus, the electron correlation, thus, reducing the phase transition temperature [11,17].

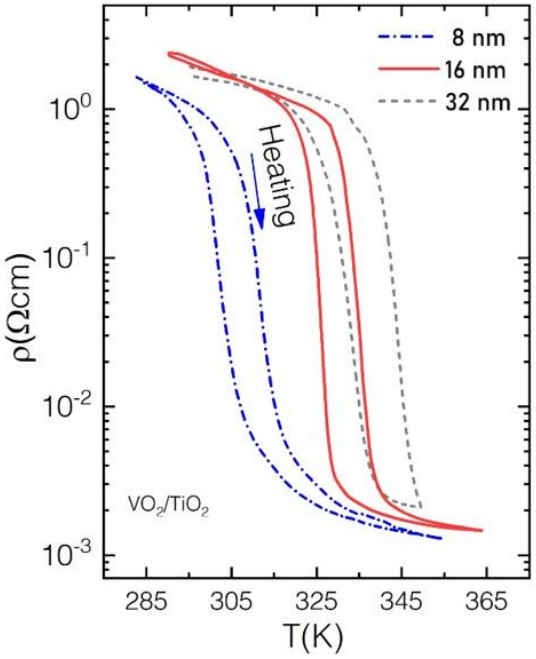

Figure A1. Temperature dependent resistive switching of the VO_2 thin films of 8 nm, 16 nm and 32 nm thickness across the heating cooling cycle.

Appendix B

In order to better visualize the different VB contributions, the variable photon energy VB spectra of the VO_2 8 nm thin film in the insulating and metallic phase are reported in Figure A2, along with the XANES spectrum.

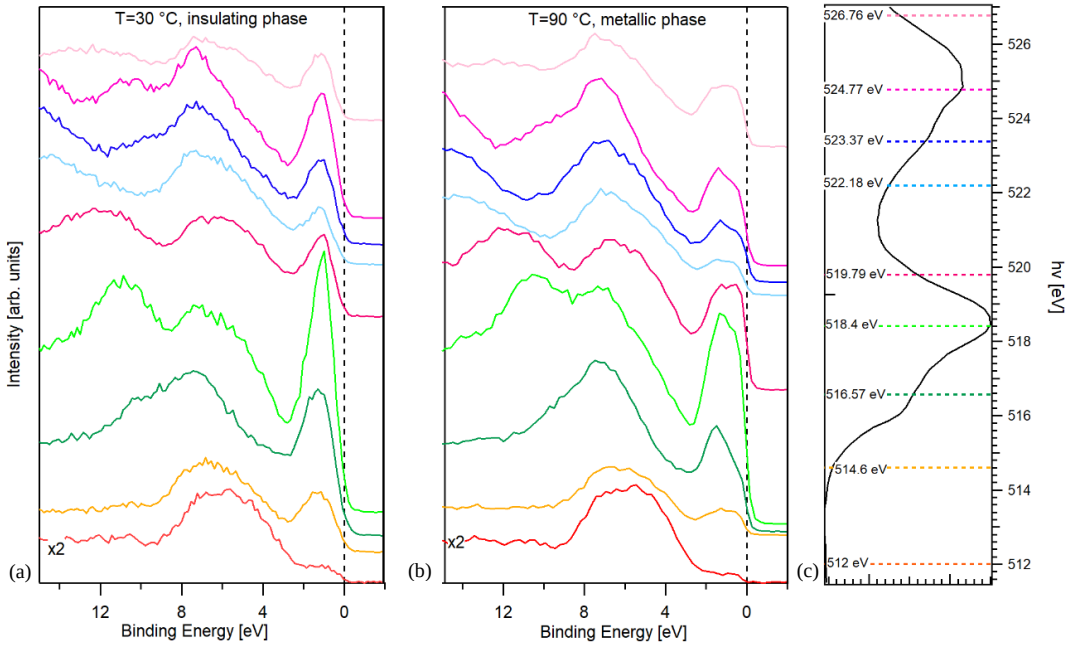

Figure A2. Variable energy Valence Band spectra of the 8 nm VO_2 film in the binding energy range (15; 1 eV). The spectra have been collected on resonance to the energy of the V L_3-edge (518.4 eV) and off resonance (512, 514.6, 516.57, 519.79, 522.18, 523.37, 524.7 and 526.76 eV) both in the insulating (T = 30 °C, (**a**)) and in the metallic phase (T = 90 °C, (**b**)). In the panel (**c**) is shown the XANES spectrum of the insulating phase (Auger yield at 464 eV). Spectra collected at 512 eV have been magnified ×2.

As observable, the metallic phase spectrum the feature centered at about 1.5 eV of BE exhibits the presence of two convoluted peaks. The one closer to FL is assigned to the C photoemission process, and the one at about 1.5 eV is assigned to the L. The V *3p* photoemission spectra is reported in Figure A3 along with its fit components.

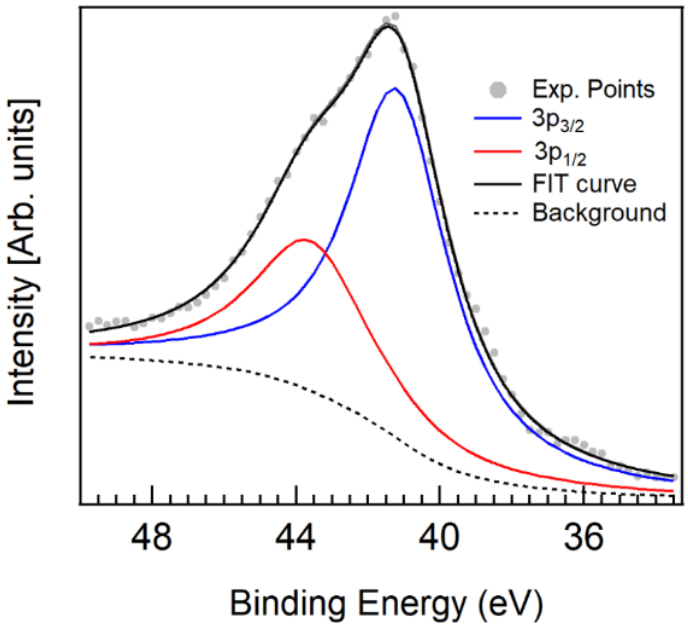

Figure A3. V *3p* XPS spectrum of the 8 nm (−24 °C) films collected at hv = 510 eV. The experimental points (grey dots) are compared to the fit components (blue $3p_{3/2}$) and (red $3p_{1/2}$) and their sum (continuous black line).

References

1. Morin, F.J. Oxides which show a metal-to-insulator transition at the neel temperature. *Phys. Rev. Lett.* **1959**, *3*, 34–36. [CrossRef]
2. Cui, Y.; Ke, Y.; Liu, C.; Chen, Z.; Wang, N.; Zhang, L.; Zhou, Y.; Wang, S.; Gao, Y.; Long, Y. Thermochromic VO_2 for Energy-Efficient Smart Windows. *Joule* **2018**, *2*, 1707–1746. [CrossRef]
3. Chen, S.; Wang, Z.; Ren, H.; Chen, Y.; Yan, W.; Wang, C.; Li, B.; Jiang, J.; Zou, C. Gate-controlled VO 2 phase transition for high-performance smart windows. *Sci. Adv.* **2019**, *5*, eaav6815. [CrossRef]
4. Kang, C.; Zhang, C.; Yao, Y.; Yang, Y.; Zong, H.; Zhang, L.; Li, M. Enhanced thermochromic properties of vanadium dioxide (VO_2)/glass heterostructure by inserting a Zr-based thin film metallic glasses (Cu50Zr50) buffer layer. *Appl. Sci.* **2018**, *8*, 1751. [CrossRef]
5. Lin, J.; Ramanathan, S.; Guha, S. Electrically driven insulator-metal transition-based devices—Part I: The Electrothermal model and experimental analysis for the dc characteristics. *IEEE Trans. Electron. Devices* **2018**, *65*, 3982–3988. [CrossRef]
6. Ramanathan, S. *Thin Film Metal-Oxides: Fundamentals and Applications in Electronics and Energy*; Springer: Boston, MA, USA, 2010; ISBN 9781441906632.
7. Brahlek, M.; Zhang, L.; Lapano, J.; Zhang, H.T.; Engel-Herbert, R.; Shukla, N.; Datta, S.; Paik, H.; Schlom, D.G. Opportunities in vanadium-based strongly correlated electron systems. *MRS Commun.* **2017**, *7*, 27–52. [CrossRef]
8. Koethe, T.C.; Hu, Z.; Haverkort, M.W.; Schüßler-Langeheine, C.; Venturini, F.; Brookes, N.B.; Tjernberg, O.; Reichelt, W.; Hsieh, H.H.; Lin, H.J.; et al. Transfer of spectral weight and symmetry across the metal-insulator transition in VO_2. *Phys. Rev. Lett.* **2006**. [CrossRef]
9. D'Elia, A.; Grazioli, C.; Cossaro, A.; Li, B.W.; Zou, C.W.; Rezvani, S.J.; Pinto, N.; Marcelli, A.; Coreno, M. Strain mediated Filling Control nature of the Metal-Insulator Transition of VO_2 and electron correlation effects in Nanostructured films. *Appl. Surf. Sci.* **2020**, 148341. [CrossRef]
10. Weber, C.; O'Regan, D.D.; Hine, N.D.M.; Payne, M.C.; Kotliar, G.; Littlewood, P.B. Vanadium Dioxide: A Peierls-Mott Insulator Stable against Disorder. *Phys. Rev. Lett.* **2012**, *108*, 256402. [CrossRef]
11. Fan, L.L.; Chen, S.; Luo, Z.L.; Liu, Q.H.; Wu, Y.F.; Song, L.; Ji, D.X.; Wang, P.; Chu, W.S.; Gao, C.; et al. Strain dynamics of ultrathin VO^2 film grown on TiO_2 (001) and the associated phase transition modulation. *Nano Lett.* **2014**, *14*, 4036–4043. [CrossRef]
12. Singh, C.N.; Piper, L.F.J.; Paik, H.; Schlom, D.G.; Lee, W. Correlation induced emergent charge order in metallic vanadium dioxide. *arXiv* **2020**, arXiv:2005.02957.
13. Aetukuri, N.B.; Gray, A.X.; Drouard, M.; Cossale, M.; Gao, L.; Reid, A.H.; Kukreja, R.; Ohldag, H.; Jenkins, C.A.; Arenholz, E.; et al. Control of the metal-insulator transition in vanadium dioxide by modifying orbital occupancy. *Nat. Phys.* **2013**, *9*, 661–666. [CrossRef]
14. Park, J.H.; Coy, J.M.; Kasirga, T.S.; Huang, C.; Fei, Z.; Hunter, S.; Cobden, D.H. Measurement of a solid-state triple point at the metal–insulator transition in VO_2. *Nature* **2013**, *500*, 431–434. [CrossRef]
15. Narayan, J.; Bhosle, V.M. Phase transition and critical issues in structure-property correlations of vanadium oxide. *J. Appl. Phys.* **2006**, *100*. [CrossRef]
16. Atkin, J.M.; Berweger, S.; Chavez, E.K.; Raschke, M.B.; Cao, J.; Fan, W.; Wu, J. Strain and temperature dependence of the insulating phases of VO_2 near the metal-insulator transition. *Phys. Rev. B Condens. Matter Mater. Phys.* **2012**, *85*, 020101. [CrossRef]
17. D'Elia, A.; Rezvani, S.J.; Cossaro, A.; Stredansky, M.; Grazioli, C.; Li, B.W.; Zou, C.W.; Coreno, M.; Marcelli, A. Strain Induced Orbital Dynamics Across the Metal Insulator Transition in Thin VO_2/TiO_2 (001) Films. *J. Supercond. Nov. Magn.* **2020**, *33*, 2383–2388. [CrossRef]
18. Lopez, R.; Haynes, T.E.; Boatner, L.A.; Feldman, L.C.; Haglund, R.F. Size effects in the structural phase transition of VO_2 nanoparticles. *Phys. Rev. B Condens. Matter Mater. Phys.* **2002**, *65*, 2241131–2241135. [CrossRef]
19. Donev, E.U.; Ziegler, J.I.; Haglund, R.F.; Feldman, L.C. Size effects in the structural phase transition of VO_2 nanoparticles studied by surface-enhanced Raman scattering. *J. Opt. A Pure Appl. Opt.* **2009**, *11*, 125002. [CrossRef]

20. Fan, L.; Wang, F.; Chen, X.; Liu, Z.; Ma, C.; Zhu, L.; Meng, Q.; Wang, B.; Zhang, Q.; Zou, C. Well-Dispersed Monoclinic VO_2 Nanoclusters with Uniform Size for Sensitive near-Infrared Detection. *ACS Appl. Nano Mater.* **2018**, *1*, 5044–5052. [CrossRef]
21. Bachrach, R.Z. *Synchrotron Radiation Research Advances in Surface and Interface Science*; Bachrach, R.Z., Ed.; Springer: Boston, MA, USA, 1992; ISBN 978-0-306-43873-8.
22. Marcelli, A.; Coreno, M.; Stredansky, M.; Xu, W.; Zou, C.; Fan, L.; Chu, W.; Wei, S.; Cossaro, A.; Ricci, A.; et al. Nanoscale Phase Separation and Lattice Complexity in VO_2: The Metal–Insulator Transition Investigated by XANES via Auger Electron Yield at the Vanadium L23-Edge and Resonant Photoemission. *Condens. Matter* **2017**, *2*, 38. [CrossRef]
23. Wu, M.; Zheng, J.C.; Wang, H.Q. Investigation of the vanadium L23 -edge X-ray absorption spectrum of $SrVO_3$ using configuration interaction calculations: Multiplet, valence, and crystal-field effects. *Phys. Rev. B* **2018**, *97*, 245138. [CrossRef]
24. Quackenbush, N.F.; Paik, H.; Wahila, M.J.; Sallis, S.; Holtz, M.E.; Huang, X.; Ganose, A.; Morgan, B.J.; Scanlon, D.O.; Gu, Y.; et al. Stability of the M2 phase of vanadium dioxide induced by coherent epitaxial strain. *Phys. Rev. B* **2016**, *94*, 085105. [CrossRef]
25. Paez, G.J.; Singh, C.N.; Wahila, M.J.; Tirpak, K.E.; Quackenbush, N.F.; Sallis, S.; Paik, H.; Liang, Y.; Schlom, D.G.; Lee, T.L.; et al. Simultaneous Structural and Electronic Transitions in Epitaxial VO_2/TiO_2 (001). *Phys. Rev. Lett.* **2020**, *124*, 196402. [CrossRef]
26. Bianconi, A. Multiplet splitting of final-state configurations in x-ray-absorption spectrum of metal VO_2: Effect of core-hole-screening, electron correlation, and metal-insulator transition. *Phys. Rev. B* **1982**, *26*, 2741–2747. [CrossRef]
27. Pinto, N.; Rezvani, S.J.; Favre, L.; Berbezier, I.; Fretto, M.; Boarino, L. Geometrically induced electron-electron interaction in semiconductor nanowires. *Appl. Phys. Lett.* **2016**, *109*, 123101. [CrossRef]
28. Rezvani, S.J.; Gunnella, R.; Neilson, D.; Boarino, L.; Croin, L.; Aprile, G.; Fretto, M.; Rizzi, P.; Antonioli, D.; Pinto, N. Effect of carrier tunneling on the structure of Si nanowires fabricated by metal assisted etching. *Nanotechnology* **2016**, *27*, 345301. [CrossRef]
29. Pasqualini, M.; Calcaterra, S.; Maroni, F.; Rezvani, S.J.; Di Cicco, A.; Alexander, S.; Rajantie, H.; Tossici, R.; Nobili, F. Electrochemical and spectroscopic characterization of an alumina-coated LiMn2O4 cathode with enhanced interfacial stability. *Electrochim. Acta* **2017**, *258*, 175–181. [CrossRef]
30. Javad Rezvani, S.; Di Gioacchino, D.; Gatti, C.; Ligi, C.; Guidi, M.C.; Cibella, S.; Fretto, M.; Poccia, N.; Lupi, S.; Marcelli, A. Proximity array device: A novel photon detector working in long wavelengths. *Condens. Matter* **2020**, *5*, 33. [CrossRef]
31. D'Elia, A.; Cepek, C.; de Simone, M.; Macis, S.; Belec, B.; Fanetti, M.; Piseri, P.; Marcelli, A.; Coreno, M. Interplay among work function, electronic structure and stoichiometry in nanostructured VO x films. *Phys. Chem. Chem. Phys.* **2020**, *22*, 6282–6290. [CrossRef]
32. Mossanek, R.J.O.; Abbate, M. Cluster model calculations with nonlocal screening channels of metallic and insulating VO_2. *Phys. Rev. B Condens. Matter Mater. Phys.* **2006**, *74*, 125112. [CrossRef]
33. Lapeyre, G.J.; Smith, R.J.; Knapp, J.; Anderson, J. Constant Final Energy and Constant Initial Energy Spectroscopy. *Le J. Phys. Colloq.* **1978**, *39*, 134–141. [CrossRef]
34. Solomon, E.I.; Basumallick, L.; Chen, P.; Kennepohl, P. Variable energy photoelectron spectroscopy: Electronic structure and electronic relaxation. *Coord. Chem. Rev.* **2005**, *249*, 229–253. [CrossRef]
35. D'Elia, A.; Grazioli, C.; Cossaro, A.; Li, B.; Zou, C.; Rezvani, J.; Pinto, N.; Marcelli, A.; Coreno, M. Electron Correlation driven Metal-Insulator transition in Strained and Disordered VO_2 films. *arXiv* **2020**, arXiv:2006.07930.
36. De Groot, F. Multiplet effects in X-ray spectroscopy. *Coord. Chem. Rev.* **2005**, *249*, 31–63. [CrossRef]
37. Goodenough, J.B. The two components of the crystallographic transition in VO_2. *J. Solid State Chem.* **1971**, *3*, 490–500. [CrossRef]
38. Sawatzky, G.A.; Post, D. X-ray photoelectron and Auger spectroscopy study of some vanadium oxides. *Phys. Rev. B* **1979**, *20*, 1546–1555. [CrossRef]
39. Ruzmetov, D.; Senanayake, S.D.; Ramanathan, S. X-ray absorption spectroscopy of vanadium dioxide thin films across the phase-transition boundary. *Phys. Rev. B Condens. Matter Mater. Phys.* **2007**, *75*. [CrossRef]

40. Cavalleri, A.; Dekorsy, T.; Chong, H.H.W.; Kieffer, J.C.; Schoenlein, R.W. Evidence for a structurally-driven insulator-to-metal transition in VO_2: A view from the ultrafast timescale. *Phys. Rev. B* **2004**, *70*, 161102. [CrossRef]
41. Schmid, M.; Steinrück, H.P.; Gottfried, J.M. A new asymmetric Pseudo-Voigt function for more efficient fitting of XPS lines. *Surf. Interface Anal.* **2014**, *46*, 505–511. [CrossRef]
42. Zimmermann, R.; Claessen, R.; Reinert, F.; Steiner, P.; Hüfner, S. Strong hybridization in vanadium oxides: Evidence from photoemission and absorption spectroscopy. *J. Phys. Condens. Matter* **1998**, *10*, 5697–5716. [CrossRef]
43. Lytken, O.; Wechsler, D.; Steinrück, H.P. Removing photoemission features from Auger-yield NEXAFS spectra. *J. Electron Spectros. Relat. Phenom.* **2017**. [CrossRef]
44. Lee, S.; Meyer, T.L.; Sohn, C.; Lee, D.; Nichols, J.; Lee, D.; Seo, S.S.A.; Freeland, J.W.; Noh, T.W.; Lee, H.N. Electronic structure and insulating gap in epitaxial VO_2 polymorphs. *APL Mater.* **2015**, *3*, 126109. [CrossRef]
45. Fan, L.L.; Chen, S.; Wu, Y.F.; Chen, F.H.; Chu, W.S.; Chen, X.; Zou, C.W.; Wu, Z.Y. Growth and phase transition characteristics of pure M-phase VO_2 epitaxial film prepared by oxide molecular beam epitaxy. *Appl. Phys. Lett.* **2013**, *103*. [CrossRef]
46. Costantini, R.; Stredansky, M.; Cvetko, D.; Kladnik, G.; Verdini, A.; Sigalotti, P.; Cilento, F.; Salvador, F.; De Luisa, A.; Benedetti, D.; et al. ANCHOR-SUNDYN: A novel endstation for time resolved spectroscopy at the ALOISA beamline. *J. Electron Spectros. Relat. Phenom.* **2018**, *229*, 7–12. [CrossRef]